

Amine-Modified SBA-15: Effect of Pore Structure on the Performance for CO₂ Capture

Xinlong Yan, Lei Zhang, Ying Zhang, Guidong Yang, and Zifeng Yan*

State Key Laboratory of Heavy Oil Processing, CNPC Key Laboratory of Catalysis, China University of Petroleum, Qingdao 266555, People's Republic of China

S Supporting Information

ABSTRACT: Several SBA-15 silica materials with different pore structures were synthesized and functionalized with poly(ethyleneimine) (PEI). The as-prepared materials were characterized by XRD, SEM, TG, FT-IR, and N₂ physisorption techniques followed by testing for CO₂ capture using a N₂ stream containing 15.1 v/v% CO₂ in the temperature range of 30–75 °C. The results showed that the CO₂ adsorption capacity linearly increased with the total pore volume of the SBA-15 phases in the tested temperature range ($R^2 > 0.94$). Temperature also showed a strong influence on CO₂ adsorption capacity. SBA-15 material with the largest pore volume (1.14 cm³ g⁻¹) exhibited the largest CO₂ adsorption capacity (105.2 mg g⁻¹ adsorbent) with 15.1 v/v% CO₂ in N₂ at 75 °C and atmospheric pressure. Pore size was found not to be the main factor influencing the CO₂ adsorption capacity of these PEI-modified SBA-15 materials. Adsorption–desorption cycles (12) revealed that the adsorbents with PEI loaded inside the pore channels were found to be quite stable, as they retained their CO₂ adsorption capacity with many cycles.

1. INTRODUCTION

Global climate change has become a worldwide issue^{1,2} because of significant and continuous rise in atmospheric CO₂ concentration by the extensive utilization of fossil fuels. Therefore, governments, industries, and academia (universities) are pursuing pathways to significantly reduce the amounts of carbon dioxide emitted into the atmosphere with the use of fossil fuels. Carbon capture and sequestration provide a critical option for meeting our basic requirements for energy while combating (and mitigating) climate change. In postcombustion capture, the most mature technology for possible, large-scale carbon dioxide capture utilized aqueous solutions of monoethanolamine (MEA),³ which selectively absorbed CO₂ around ambient conditions (40–65 °C, 1 atm). The concentrated CO₂ was then recovered, and the solvent was regenerated by heating to temperatures well above 100 °C. The energy (along with the capital and operating costs) required for solvent regeneration became a major barrier for its application for capturing CO₂ by retrofitting coal-fired power plants as well as other major CO₂ emitting industries. Separation and capture of CO₂ from flue gas streams is probably the most difficult and expensive process. Therefore, there is a great need to develop viable and cost-effective technologies for postcombustion CO₂ capture.

CO₂ capture by adsorption is one promising method. Recently, aqueous amines immobilized in/on mesoporous silica adsorbents have attracted considerable attention due to their high efficiency and selectivity for CO₂ capture from a gas mixture.^{4,5} Specifically, ordered mesoporous materials offer structural characteristics such as large pore size, high surface area, and a large number of highly dispersed active sites on the pore surface, which facilitate the distribution of amines throughout the pore space, thereby promoting the CO₂ adsorption

capacity of the adsorbents.⁶ There are two main preparation methods to obtain the supported amine sorbents:⁵ (i) porous supports impregnated with liquid organic polymer such as poly(ethyleneimine) (PEI) via the wet impregnation method and (ii) amines that could be covalently linked to a solid support via the use of silane chemistry. “Wet impregnation” of mesoporous silica with amines could be a simple method to obtain a high capacity adsorbent.

The type of porous silica support was found to play a vital role in the performance of these adsorbents. Various mesoporous silica materials such as MCM-41,^{6,7} MCM-48,^{8–11} pore expanded MCM-41,^{12,13} SBA-12,¹⁴ SBA-15,^{15–24} SBA-16,^{25,26} HMS,²⁷ mesoporous silica microspheres,²⁸ and mesocellular silica foam²⁹ were investigated. Ahn et al³⁰ modified a series of mesoporous silica materials (MCM-41, MCM-48, SBA-15, SBA-16, and KIT-6) with 50 wt % PEI to evaluate the CO₂ adsorption performance of these materials. They found that equilibrium adsorption capacity of CO₂ increased with increasing average pore diameter of the bare support. Moreover, it was interesting to note that even though MCM-48 and SBA-16 possessed three-dimensional pore interconnectivity, their CO₂ adsorption capacities were not better than those of one-dimensional supports such as SBA-15. Zelenák et al³¹ prepared MCM-41, SBA-12 and SBA-15 mesoporous silica materials, and these materials were functionalized with aminopropyl (AP) ligands for CO₂ capture. They also found that the sorption capacity depended on the pore size of the mesoporous silica. However, it was unclear from these

Received: June 8, 2010

Accepted: January 13, 2011

Revised: December 16, 2010

Published: February 15, 2011

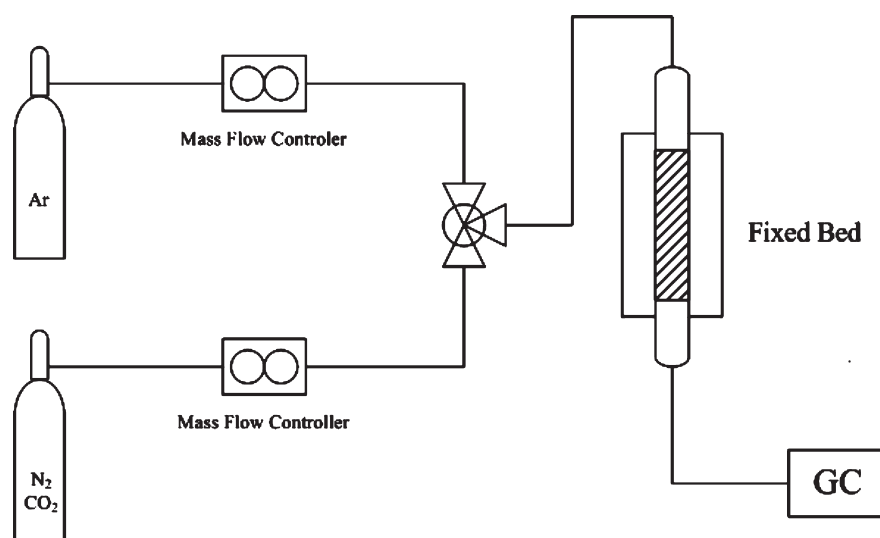


Figure 1. Diagram of fixed bed setup for the CO₂ capture.

studies whether the CO₂ adsorption capacity was merely dependent on the pore diameter of the support materials⁵ or related to other unique properties of these materials.

Compared to other mesoporous materials, SBA-15 was found to be one of the most suitable substrates for CO₂ capture by modification due to its large pore volume and pore diameter.^{30–32} In addition, the intrawall pores of SBA-15 form a continuous network that connects adjacent main channels, which would be beneficial for the mass transfer during adsorption. In the present work, several SBA-15 support materials with different structural properties were prepared followed by their impregnation with PEI. The obtained samples were characterized by XRD, N₂ physisorption technique, SEM, TG, and Fourier transform infrared (FT-IR) spectroscopy. The effect of pore size and total porosity on the CO₂ adsorption capacity and thermal stability were discussed.

2. EXPERIMENTAL SECTION

2.1. Preparation and Functionalization of SBA-15. The SBA-15 materials with different pore diameters were synthesized based on the method reported by Fulvio et al.³³ In a typical synthesis, 8.0 g of Pluronic 123 was added to 288 mL of 1.7 M HCl solution and stirred for 4 h at 40 °C, followed by adding 16.5 g of TEOS and stirring for another 2 h. The synthesized gel was hydrothermally heated at 100 °C for different times ranging from 6 to 48 h under static conditions. The as-synthesized samples were recovered by filtration and dried at room temperature. The template was then removed by calcination in air at 550 °C for 6 h. The samples obtained were denoted as S-*x*, where *x* represented the time of the hydrothermal treatment process.

SBA-15 with interconnecting 3D large-pore networks was prepared by following the procedure reported previously.³⁴ Briefly, 4.0 g of Pluronic 123 was dissolved in 150 mL of 1.7 M HCl solution at 40 °C, and then 8.2 g of TEOS was added. After 24 h stirring at 40 °C, the milky mixture was aged at 130 °C for 24 h under static conditions. The calcined 3D sample was obtained as described above, and this sample was designated as S-3D.

PEI-functionalized SBA-15 materials were prepared by wet impregnation, according to the procedure reported in the literature.³⁵ In a typical preparation, 1.5 g of PEI (Aldrich,

average molecular weight 423, linear type, bp 250 °C) was dissolved in 12.0 g of methanol under stirring for 30 min, and then 1.5 g of calcined SBA-15 (S-*x*) was added to the mixture. The resulting slurry was stirred at room temperature for 6 h, dried at 90 °C for >6 h, and labeled as S-*x*/P materials.

2.2. Characterization. Powder XRD patterns of all samples were recorded on a Panalytical Xpert PRO X-ray diffractometer with Cu K α radiation ($\lambda = 0.15406$ nm, 40 kV, 40 mA). The unit cell parameter *a* was calculated from the (100) diffraction peak according to the equation: $a = 2 \times d_{100}/3^{1/2}$. The N₂ adsorption–desorption isotherms were collected at 77 K using Micromeritics TriStar 3000 Porosimeter. The adsorbent was degassed prior to each measurement at 100 °C in a high vacuum for 3 h. The surface area was calculated using the BET method. The total pore volume was determined as the volume of liquid nitrogen adsorbed at a relative pressure of 0.99. The volume of intrawall pores and pore size were obtained using NLDFT methods from the adsorption branch^{36,37} as implemented in Micromeritics Instrument Corporation's data software DFT plus(R) V3.00. FT-IR spectra were recorded using a Nicolet MAGNA 750 Spectrometer by measuring the absorbance of the KBr pellet containing 1–2 wt % of sample. The spectra were collected in the range of 4000–400 cm⁻¹ after 32 scans at a resolution of 4 cm⁻¹. The thermogravimetric analysis (TGA) was performed on a Netzsch STA 449C thermogravimetric analyzer with a temperature ramp of 20 K min⁻¹ in air. SEM investigation of morphological features was carried out using a Hitachi S-4800 instrument.

2.3. CO₂ Capture. CO₂ capture was performed in a homemade fixed bed reactor (Figure 1) operated at atmospheric pressure. In the reactor, 1.0 g of a dried adsorbent was packed into the bed in the middle of the reactor supported with quartz wool. Prior to each adsorption measurement, the adsorbent was first activated by heating at 100 °C for 1 h in Ar stream at a flow rate of 75 mL min⁻¹. After cooling to the desired adsorption temperature, an N₂ stream containing 15.1 v/v% CO₂ at a total flow rate of 10 mL min⁻¹ was introduced and passed through the adsorbent. The CO₂ concentration in the influent and effluent gas streams were analyzed with an online gas chromatograph (Agilent 6820) equipped with a thermal conductivity detector (TCD) and Porapak-Q packed column. The adsorption capacity

Table 1. Structure Property of the Unmodified and Modified SBA-15 Samples

	a_0	BET surface area (m^2g^{-1})	total pore volume (cm^3g^{-1})	intrawall pore volume (cm^3g^{-1})	pore diameter (nm)	wall thickness (nm)	sorption capacity at 75 °C ($\text{mg g}^{-1}\text{adsorbent}$)
S-6	10.7	761.2	0.71	0.11	6.9	3.8	—
S-24	11.9	893.9	1.06	0.2	8.5	3.3	—
S-48	11.6	802.9	1.14	0.2	8.6	3.0	—
S-3D	11.8	556.3	0.99	0.08	9.4	2.4	—
S-6/P	10.6	—	—	—	—	—	82.4
S-24/P	11.9	26.5	0.07	0	3.7	8.2	99.3
S-48/P	11.8	46	0.11	0	4.9	6.9	105.2
S-3D/P	11.6	27.6	0.07	0	3.3	8.3	92.2

of CO_2 on an adsorbent (Q , mg g^{-1}) was calculated as

$$Q = \frac{F \times M \times \int_0^t (C_0 - C_t) dt}{W}$$

where t was the sorption time (min), F was the flow rate (mmol min^{-1}), M was the molecular weight (g mol^{-1}) of CO_2 , W was the weight of sorbent (g), and C_0 and C_t were the influent and effluent CO_2 concentrations (mg L^{-1}), respectively. Several CO_2 adsorption–desorption cycles were conducted on the same sample for testing its stability to capture CO_2 .

3. RESULTS AND DISCUSSION

3.1. PEI Impregnated into SBA-15 Substrates. Textural properties of all the samples prepared in this work are summarized in Table 1. It can be seen that the S-6 had the lowest total pore volume ($0.71\text{ cm}^3\text{g}^{-1}$) and pore size (6.9 nm), and a significant volume of intrawall pores of $0.11\text{ cm}^3\text{g}^{-1}$. By further increasing the hydrothermal treatment time to 24 h, the total pore volume and pore size of S-24 increased from 0.71 to $1.06\text{ cm}^3\text{g}^{-1}$ and 6.9 to 8.5 nm, respectively. The volume of intrawall pores also increased to $0.2\text{ cm}^3\text{g}^{-1}$. For the S-48 sample, the total pore volume and pore size were $1.14\text{ cm}^3\text{g}^{-1}$ and 8.6 nm, respectively, and the volume of intrawall pores was unchanged compared with that of S-24. S-3D had the largest pore size of 9.4 nm among the four samples with a pore volume of $0.99\text{ cm}^3\text{g}^{-1}$ and intrawall pore volume of $0.08\text{ cm}^3\text{g}^{-1}$.

After 50% PEI loading, the mesoporous structures of the silica materials were preserved. However, the peak intensity in the XRD patterns became less prominent compared with those of pure support materials (Supporting Information, Figure S1). The N_2 adsorption capacity of all the samples was found to decrease significantly. The adsorption isotherms of S-24/P, S-48 h/P, and S-3D/P maintained the typical type IV isotherm shape. However, the S-6 sample showed no nitrogen gas adsorption (Supporting Information, Figure S2). Therefore, information on the meaningful textural properties could not be obtained from the N_2 adsorption–desorption isotherms of PEI loaded samples. For S-24/P material, the specific BET surface area was only $26.5\text{ m}^2\text{g}^{-1}$ with a pore volume of $0.07\text{ cm}^3\text{g}^{-1}$. Similar to S-24/P, the BET surface areas of S-48/P and S-3D/P decreased to $46\text{ m}^2\text{g}^{-1}$ and $27.6\text{ m}^2\text{g}^{-1}$ and pore volumes decreased to $0.11\text{ m}^3\text{g}^{-1}$ and $0.07\text{ m}^3\text{g}^{-1}$, respectively. It appears that the intrawall pores of all the SBA-15 samples were totally filled up with PEI. SEM pictures showed that the S-24/P, S-48/P, and S-3D/P samples still retained their original morphology. However, the loading amount of PEI in S-6/P was in excess of its maximum adsorption

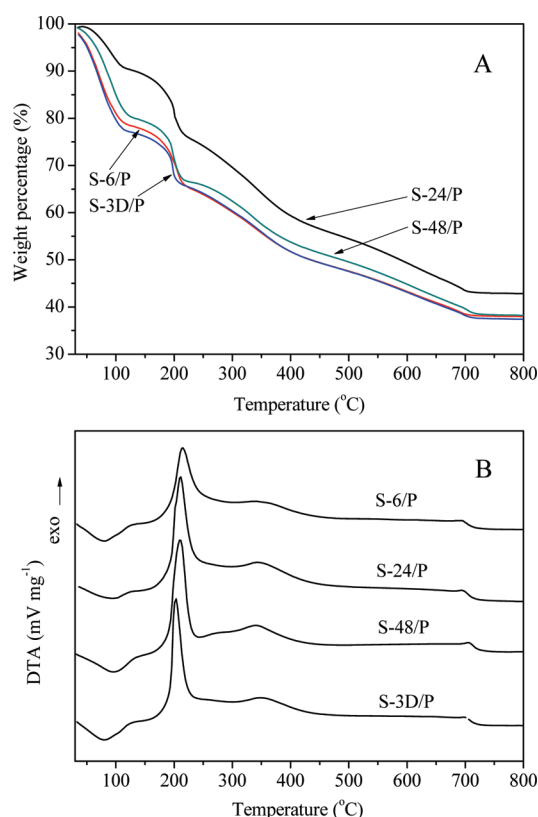


Figure 2. TG (A) and DTA (B) profiles of PEI impregnated SBA-15 samples.

capacity, because PEI was coated on the external surfaces of the mesoporous materials as could be observed in SEM picture (Supporting Information, Figure S3). All the characterization results (XRD, N_2 physisorption and SEM) indicated that the PEI was loaded inside the pore channels of these porous materials.

The amount of PEI loaded into the porous substrates by impregnation method was measured by thermogravimetry. Figure 2 shows the weight loss by TGA and differential thermal analysis (DTA) profiles of PEI-impregnated SBA-15 samples. From the DTA curves, two main exothermic peaks and one endothermic peak could be seen, corresponding to four weight loss regions in the TG curves. The first step of the thermal decomposition occurred at a temperature of about 100 °C. This could be attributed to desorption of moisture and CO_2 . In the temperature range of 140–700 °C, two exothermic peaks

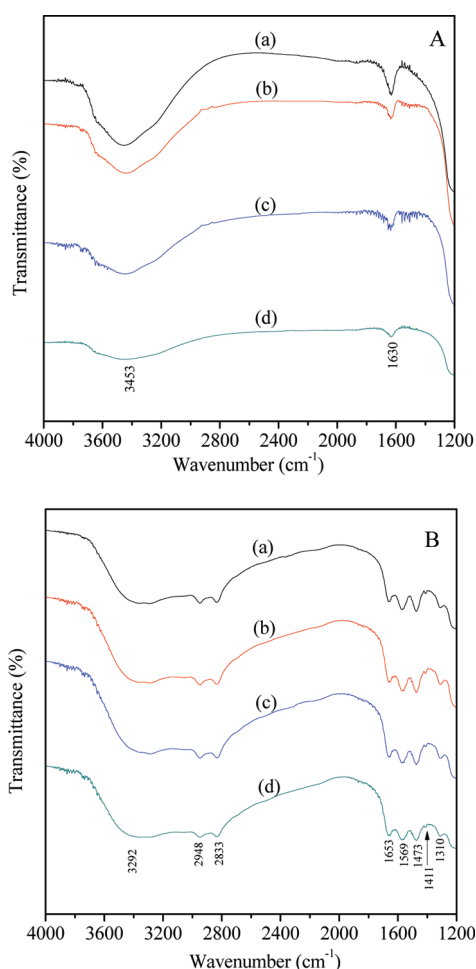


Figure 3. FT-IR spectra of SBA-15 substrates and PEI functionalized SBA-15 samples. A: (a) S-6, (b) S-24, (c) S-48, (d) S-3D; B: (a) S-6/P, (b) S-24/P, (c) S-48/P, (d) S-3D/P.

appeared at about 200 and 350 °C and these could be primarily ascribed to the combustion of the organic materials. The total weight losses of S-6/P, S-24/P, S-48/P, and S-3D/P were 61.5%, 56.5%, 60.4%, and 61.8%, respectively, in the temperature range of 32–700 °C. If the adsorbed moisture and CO₂ were excluded from the total weight, the loading amount of PEI on the four SBA-15 substrates could be calculated to be about 50 wt %. The results confirmed that virtually identical amounts of PEI were loaded into the mesoporous silica materials and apparently no PEI loss occurred during the impregnation process.

Note that PEI was not simply loaded on SBA-15 through physical interaction only.³² The IR spectra of SBA-15 substrates and PEI functionalized SBA-15 samples are shown in Figure 3. The spectra of all of the samples were recorded by IR spectrometer without any pretreatment. All SBA-15 substrates exhibited rather similar spectra (Figure 3A) with an FT-IR band around 3453 cm⁻¹. This band could be assigned to the O–H stretching vibrations of the hydrogen-bonded silanol groups and adsorbed water molecules. The band located at 1630 cm⁻¹ was attributed to adsorbed water. After PEI loading, these bands corresponding to O–H bending and adsorbed water were not observed in the IR spectra (Figure 3B), indicating that the isolated surface hydroxyl groups of SBA-15 materials reacted with the amine groups in PEI possibly forming Si–O⁻N⁺H₃R and/or Si–O⁻N⁺H₂R groups.³²

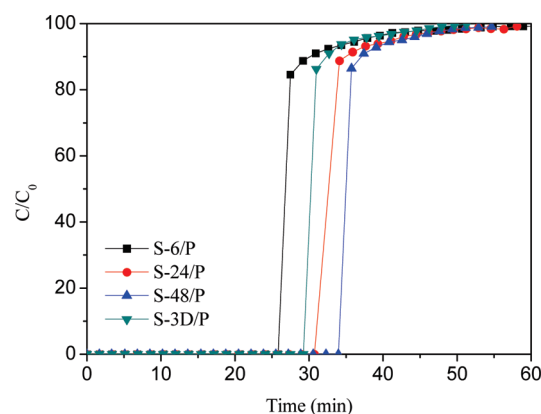
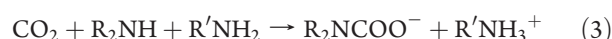


Figure 4. Adsorption breakthrough curves for CO₂ using a gas mixture with 15.1% v/v CO₂ in N₂ over functionalized SBA-15 samples at 75 °C.

Some additional bands could be observed in the FT-IR spectra of modified SBA-15 samples (Figure 3B) compared to those of unmodified SBA-15. The broad band appearing at 3292 cm⁻¹ could be attributed to the amine N–H stretching vibrations. Two distinctly new bands appeared at 2948 and 2833 cm⁻¹, which were due to the CH₂ stretching modes of the PEI chains. Two other IR bands appeared at 1569 and 1473 cm⁻¹, which could be characteristics of the asymmetric and symmetric bending of primary amines (NH₂), respectively. The bands observed at 1633 cm⁻¹ in the four IR spectra could be assigned to the bending of secondary amines [N(R)H] in PEI.³⁸ In addition, the bands at 1411 and 1310 cm⁻¹ could be ascribed to NCOO skeletal vibration.³⁹

The chemical reaction between amine and CO₂ could result in the formation of ammonium carbamates under anhydrous conditions through the following equations:^{39,40}



In the presence of water, the interaction between amine and CO₂ yielded ammonium bicarbonate which involved the following steps:^{41,42}



where R was an alkyl group and CO₂ could also react with H₂O to produce HCO₃⁻ and CO₃²⁻.

3.2. Effect of Pore Structure on CO₂ Adsorption Capacity. Depending on the types of fuels and the combustion conditions, the conventional coal-fired power plants produce flue gas streams with CO₂ concentration of 12% to 15%. Therefore, a simulated flue gas containing 15.1 v/v % CO₂ and 84.9 v/v % N₂ was used for CO₂ adsorption test in this study. Figure 4 shows the breakthrough curves for adsorption of CO₂ on various SBA-15 materials with the same PEI loading of 50 wt % and a temperature of 75 °C. Data in Figure 4 showed that all the samples exhibited high CO₂ adsorption capacity. After 40 min of adsorption, the quantity of adsorbed CO₂ was above 80 mg g⁻¹ of adsorbent in all cases. However, the final amounts of CO₂ adsorbed were in a range of 80–110 mg g⁻¹ of adsorbent and the order of adsorption of different samples was as follows: S-6/P < S-3D/P < S-24/P < S-48/P (Table 1; Figure 4).

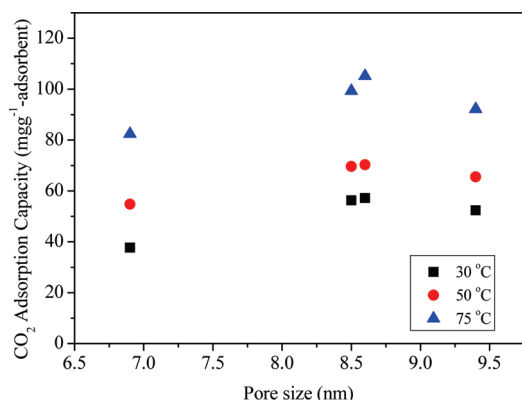


Figure 5. Relationship between the pore size of the substrates and CO₂ capture capacity.

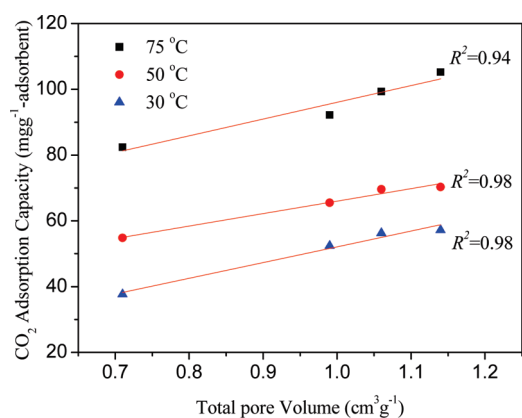


Figure 6. Correlations of total pore volume of the SBA-15 substrates and CO₂ capture at 75, 50, and 30 °C.

To investigate the effect of textural properties of SBA-15 substrates on CO₂ adsorption capacity, the relationship of CO₂ adsorption capacity versus the values of pore size and total pore volume were plotted for temperatures from 30 to 75 °C (Figures 5 and 6).

The adsorption capacities of CO₂ at 75 °C were much higher than those at 50 and 30 °C for the SBA-15 materials tested here with different pore sizes. The greater adsorption at 75 °C was probably because of the increased diffusion of the adsorbed CO₂ from the exposed surface of PEI into the bulk PEI at a higher temperature.³² The S-3D/P sample with the 3D pore architecture showed relatively lower CO₂ capacity ($Q = 92.2 \text{ mg g}^{-1}$ adsorbent) compared to the capacities of S-24/P and S-48/P (Table 1; Figure 4). This result is consistent with the work of Ahn et al.,³⁰ who found that 3D pore arrangement in mesoporous silica materials such as MCM-48 enhanced CO₂ adsorption kinetics rather than adsorption capacity. They found that the adsorption capacity increased in the order KIT-6 > SBA-16 \approx SBA-15 > MCM-48 > MCM-41, which was a function of the pore diameter of the support. However, in this study we did not find a correlation between the pore size of SBA-15 and its CO₂ adsorption capacity at all the temperatures tested here (Figure 5). The CO₂ adsorption capacity, on the other hand, increased with an increase in total pore volume of the support materials at all temperatures tested here, i.e., a linear relationship between the CO₂ adsorption capacity and total pore volume was observed (Figure 6). At all temperatures, “best-fit” straight lines

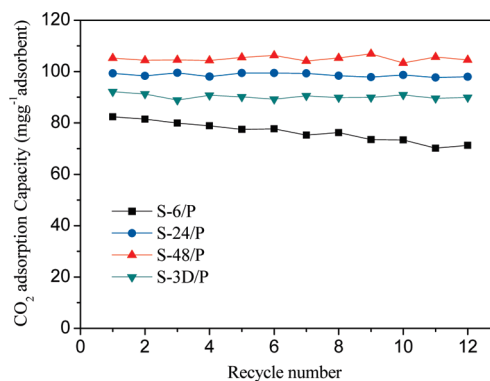


Figure 7. Recycle adsorption/desorption runs of S-6/P, S-24/P, S-48/P, and S-3D/P (adsorption at 75 °C; desorption at 100 °C).

could be drawn through the data (Figure 6). Linear regression analysis indicated that the correlation coefficient R^2 was 0.94 at 75 °C, while the R^2 was 0.98 for both 50 and 30 °C (Figure 6). This result suggested that the PEI inside the pores of the substrates was mainly responsible for CO₂ capture, and this hypothesis is consistent with the “molecular basket” theory. The mechanism of CO₂ capture in detail is as follows: PEI was anchored on the inner pore surfaces of molecular vessels such as SBA-15 to increase the accessible sorption sites and to improve the mass transfer rate in the adsorption/desorption process by increasing the gas–PEI interface. However, the PEI coated on the external surfaces of SBA-15 substrates had low efficiency to capture CO₂.⁶ Moreover, since the density of PEI is about 1.0 g mL^{-1} , the largest amount of PEI that could be theoretically loaded into the pores of 1.0 g of S-3D is 1.0 mL, that is, 50 wt % PEI loading. When the total pore volume increased from 0.99 (S-3D) to $1.06 \text{ cm}^3 \text{ g}^{-1}$ (S-24) (Table 1), the captured amount of CO₂ also increased. In addition, the maximum CO₂ adsorption capacity was observed on S-48 h/P, which had the largest pore volume ($1.14 \text{ cm}^3 \text{ g}^{-1}$). This result indicated that the fully filled “basket” was not the most suitable case for CO₂ capture. More spaces in the “basket” could enhance the amount of CO₂ capture.

3.3. Regenerability and Stability of Adsorbents. An industrially useful adsorbent should possess excellent regenerability and stability with many adsorption–desorption cycles. In order to test the stability of the adsorbents, 12 cycles of sorption–desorption were carried out. Figure 7 shows the measured sorption capacity of four adsorbents for CO₂ as a function of the number of the sorption–desorption cycles. The results showed that the performance of S-24/P, S-48/P, and S-3D/P adsorbents was fairly stable, with only a slight decrease in capacity. However, the cyclic performance of S-6/P was not as good as the others (Figure 7), as its adsorption capacity decreased very quickly with each cycle (11.1 mg g^{-1} after 12 cycles, i.e., a decrease of 13.5% of initial capacity), which might be attributed to some loss of PEI coated on the surface of S-6.

4. CONCLUSIONS

Four SBA-15 materials with different porous properties were prepared and functionalized with 50% PEI for CO₂ capture. All the PEI-loaded samples exhibited good CO₂ adsorption ability. The results indicated that the CO₂ adsorption capacity was dependent on the adsorption temperature and the total pore volume of the SBA-15 substrate. As the adsorption temperature

was increased from 30 to 75 °C, more CO₂ was adsorbed. The CO₂ adsorption amount increased proportionally with the total pore volume of the support in the temperature range examined ($R^2 > 0.94$), with the maximum CO₂ adsorption amount (105.2 mg g⁻¹ adsorbent) achieved on S-48/P that had the largest pore volume (1.14 cm³ g⁻¹) under the conditions tested here. The 12 adsorption–desorption cycle experiments revealed that the adsorbents prepared using the substrates with large pore volume exhibited only a minor drop in CO₂ capacity.

■ ASSOCIATED CONTENT

S Supporting Information. (i) XRD spectra of SBA-15 and functionalized SBA-15; (ii) N₂ adsorption–desorption isotherms and pore size distribution of unmodified and PEI-modified SBA-15 samples; (iii) SEM images of the adsorbents. This material is available free of charge via the Internet at <http://pubs.acs.org>.

■ AUTHOR INFORMATION

Corresponding Author

*Tel: 86 532 86981296. E-mail: zfyancat@upc.edu.cn.

■ ACKNOWLEDGMENT

This work is supported financially by the National Natural Science Foundation of China (Grant No. 50901090).

■ REFERENCES

- (1) Idem, R.; Tontiwachwuthikul, P. Preface for the Special Issue on the Capture of Carbon Dioxide from Industrial Sources: Technological Developments and Future Opportunities. *Ind. Eng. Chem. Res.* **2006**, *45*, 2413.
- (2) Song, C. S. Global Challenges and Strategies for Control, Conversion and Utilization of CO₂ for Sustainable Development involving Energy, Catalysis, Adsorption and Chemical Processing. *Catal. Today* **2006**, *115*, 2.
- (3) Kohl, A. L.; Nielson, R. B. *Gas Purification*; Gulf Publishing: Houston, TX, 1997.
- (4) Chew, T. L.; Ahmad, A. L.; Bhatia, S. Ordered Mesoporous Silica (OMS) as an Adsorbent and Membrane for Separation of Carbon Dioxide (CO₂). *Adv. Colloid Interface Sci.* **2010**, *153*, 43.
- (5) Choi, S.; Drese, J. H.; Jones, C. W. Adsorbent Materials for Carbon Dioxide Capture from Large Anthropogenic Point Sources. *ChemSusChem* **2009**, *2*, 796.
- (6) Xu, X. C.; Song, C. S.; Andresen, J. M.; Miller, B. G.; Scaroni, A. W. Novel Polyethylenimine-Modified Mesoporous Molecular Sieve of MCM-41 Type as High-Capacity Adsorbent for CO₂ Capture. *Energy Fuels* **2002**, *16*, 1463.
- (7) Belmabkhout, Y.; Serna-Guerrero, R.; Sayari, A. Adsorption of CO₂ from Dry Gases on MCM-41 Silica at Ambient Temperature and High Pressure. I: Pure CO₂ Adsorption. *Chem. Eng. Sci.* **2009**, *64*, 3721.
- (8) Huang, H. Y.; Yang, R. T.; Chinn, D.; Munson, C. L. Amine-Grafted MCM-48 and Silica Xerogel as Superior Sorbents for Acidic Gas Removal from Natural Gas. *Ind. Eng. Chem. Res.* **2003**, *42*, 2427.
- (9) Kim, S.; Ida, J.; Gulians, V. V.; Lin, J. Y. S. Tailoring Pore Properties of MCM-48 Silica for Selective Adsorption of CO₂. *J. Phys. Chem. B* **2005**, *109*, 6287.
- (10) Jang, H. T.; Park, Y. K.; Ko, Y. S.; Lee, J. Y. Bhagiyalakshmi Margandan. Highly Siliceous MCM-48 from Rice Husk Ash for CO₂ Adsorption. *Int. J. Greenhouse Gas Control* **2009**, *3*, 545.

(11) Bhagiyalakshmi, M.; Yun, L. J.; Anuradha, R.; Jang, H. T. Utilization of Rice Husk Ash as Silica Source for the Synthesis of Mesoporous Silicas and Their Application to CO₂ Adsorption Through TREN/TEPA Grafting. *J. Hazard. Mater.* **2010**, *175*, 928.

(12) Franchi, R. S.; Harlick, P. J. E.; Sayari, A. Applications of Pore-Expanded Mesoporous Silica. 2. Development of a High-Capacity, Water-Tolerant Adsorbent for CO₂. *Ind. Eng. Chem. Res.* **2005**, *44*, 8007.

(13) Serna-Guerrero, R.; Belmabkhout, Y.; Sayari, A. Further Investigations of CO₂ Capture using Triamine-grafted Pore-expanded Mesoporous Silica. *Chem. Eng. J.* **2010**, *158*, 513.

(14) Zelenak, V.; Halamova, D.; Gaberova, L.; Bloch, E.; Llewellyn, P. Amine-modified SBA-12 Mesoporous Silica for Carbon Dioxide Capture: Effect of Amine Basicity on Sorption Properties. *Microporous Mesoporous Mater.* **2008**, *116*, 358.

(15) Khatri, R. A.; Chuang, S. S. C.; Soong, Y.; Gray, M. M. Carbon Dioxide Capture by Diamine-Grafted SBA-15: A Combined Fourier Transform Infrared and Mass Spectrometry Study. *Ind. Eng. Chem. Res.* **2005**, *44*, 3702.

(16) Fadhel, B.; Hearn, M.; Chaffee, A. CO₂ Adsorption by PAMAM Dendrimers: Significant Effect of Impregnation into SBA-15. *Microporous Mesoporous Mater.* **2009**, *123*, 140.

(17) Liu, X.; Zhou, L.; Fu, X.; Sun, Y.; Su, W.; Zhou, Y. Adsorption and Regeneration Study of The Mesoporous Adsorbent SBA-15 Adapted to the Capture/separation of CO₂ and CH₄. *Chem. Eng. Sci.* **2007**, *62*, 1101.

(18) Chang, F. Y.; Chao, K. J.; Cheng, H. H.; Tan, C. S. Adsorption of CO₂ onto Amine-grafted Mesoporous Silicas. *Sep. Purif. Technol.* **2009**, *70*, 87.

(19) Hiyoshi, N.; Yogo, K.; Yashima, T. Adsorption Characteristics of Carbon Dioxide on Organically Functionalized SBA-15. *Microporous Mesoporous Mater.* **2005**, *84*, 357.

(20) Gray, M. L.; Soong, T. Y.; Champagne, K. J.; Pennline, H.; Baltrus, J. P.; Stevens, R. W., Jr.; Khatri, R.; Chuang, S. S. C.; Filburn, T. Improved Immobilized Carbon Dioxide Capture Sorbents. *Fuel Process. Technol.* **2005**, *86*, 1449.

(21) Zheng, F.; Tran, D. N.; Busche, B. J.; Fryxell, G. E. R.; Addleman, S.; Zemanian, T. S.; Aardahl, C. L. Ethylenediamine-Modified SBA-15 as Regenerable CO₂ Sorbent. *Ind. Eng. Chem. Res.* **2005**, *44*, 3099.

(22) Liang, Z. J.; Fadhel, B.; Schneider, C. J.; Chaffee, A. L. Stepwise Growth of Melamine-based Dendrimers into Mesopores and Their CO₂ Adsorption Properties. *Microporous Mesoporous Mater.* **2008**, *111*, 536.

(23) Rosenholm, J. M.; Penninkangas, A.; Lindén, M. Amino-functionalization of Large-pore Mesoscopically Ordered Silica by a One-step Hyperbranching Polymerization of a Surface-grown Polyethyleneimine. *Chem. Commun.* **2006**, 3909.

(24) Yue, M. B.; Chun, Y.; Cao, Y.; Dong, X.; Zhu, J. H. CO₂ Capture by As-Prepared SBA-15 with an Occluded Organic Template. *Adv. Funct. Mater.* **2006**, *16*, 1717.

(25) Wei, J. W.; Shi, J. J.; Pan, H.; Zhao, W.; Ye, Q.; Shi, Y. Adsorption of Carbon Dioxide on Organically Functionalized SBA-16. *Microporous Mesoporous Mater.* **2008**, *116*, 394.

(26) Knöfel, C.; Descarpentries, J.; Benzaouia, A.; Zelenák, V.; Mornet, S.; Llewellyn, P. L.; Hornebecq, V. Functionalised Micro-/mesoporous Silica for the Adsorption of Carbon Dioxide. *Microporous Mesoporous Mater.* **2007**, *99*, 79.

(27) Knowles, G. P.; Delaney, S. W.; Chaffee, A. L. Diethylenetriamine[propyl(silyl)]-Functionalized (DT) Mesoporous Silicas as CO₂ Adsorbents. *Ind. Eng. Chem. Res.* **2006**, *45*, 2626.

(28) Araki, S.; Doi, H.; Sano, Y.; Tanaka, S.; Miyake, Y. Preparation and CO₂ Adsorption Properties of Aminopropyl-functionalized Mesoporous Silica Microspheres. *J. Colloid Interface Sci.* **2009**, *339*, 382.

(29) Liu, S. H.; Wu, C. H.; Lee, H. K.; Liu, S. B. Highly Stable Amine-modified Mesoporous Silica Materials for Efficient CO₂ Capture. *Top Catal.* **2010**, *53*, 210.

(30) Son, W. J.; Choi, J. S.; Ahn, W. S. Adsorptive Removal of Carbon Dioxide using Polyethyleneimine-loaded Mesoporous Silica Materials. *Microporous Mesoporous Mater.* **2008**, *113*, 31.

(31) Zeleňák, V.; Badaničová, M.; Halamová, D.; Čejka, J.; Zukal, A.; Murafa, N.; Goerigk, G. Amine-modified Ordered Mesoporous Silica: Effect of Pore Size on Carbon Dioxide Capture. *Chem. Eng. J.* **2008**, *144*, 336.

(32) Ma, X. L.; Wang, X. X.; Song, C. S. Molecular Basket Sorbents for Separation of CO₂ and H₂S from Various Gas Streams. *J. Am. Chem. Soc.* **2009**, *131*, 5777.

(33) Fulvio, P. F.; Pikus, S.; Jaroniec, M. Tailoring Properties of SBA-15 Materials by Controlling Conditions of Hydrothermal Synthesis. *J. Mater. Chem.* **2005**, *15*, 5049.

(34) Fan, J.; Yu, C. Z.; Wang, L. M.; Tu, B.; Zhao, D. Y.; Sakamoto, Y.; Terasaki, O. Mesotunnels on the Silica Wall of Ordered SBA-15 to Generate Three-Dimensional Large-Pore Mesoporous Networks. *J. Am. Chem. Soc.* **2001**, *123*, 12113.

(35) Wang, X. X.; Ma, X. L.; Xu, X. C.; Sun, L.; Song, C. S. Mesoporous-molecular-sieve-supported Polymer Sorbents for Removing H₂S from Hydrogen Gas Streams. *Top Catal.* **2008**, *49*, 108.

(36) Ravikovitch, P. I.; Neimark, A. V. Characterization of Micro- and Mesoporosity in SBA-15 Materials from Adsorption Data by the NLDFT Method. *J. Phys. Chem. B* **2001**, *105*, 6817.

(37) Ravikovitch, P. I.; Neimark, A. V. Calculations of Pore Size Distributions in Nanoporous Materials from Adsorption and Desorption Isotherms. *Stud. Surf. Sci. Catal.* **2000**, *129*, 597.

(38) Wang, X. X.; Ma, X. L.; Sun, L.; Song, C. S. A Nanoporous Polymeric Sorbent for Deep Removal of H₂S from Gas Mixtures for Hydrogen Purification. *Green Chem.* **2007**, *9*, 695.

(39) Wang, X. X.; Schwartz, V.; Clark, J. C.; Ma, X. L.; Overbury, S. H.; Xu, X. C.; Song, C. S. Infrared Study of CO₂ Sorption over "Molecular Basket" Sorbent Consisting of Polyethylenimine-Modified Mesoporous Molecular Sieve. *J. Phys. Chem. C* **2009**, *113*, 7260.

(40) Hiyoshi, N.; Yogo, K.; Yashima, T. Adsorption Characteristics of Carbon Dioxide on Organically Functionalized SBA-15. *Microporous Mesoporous Mater.* **2005**, *84*, 357.

(41) Chang, A. C. C.; Chuang, S. S. C.; Gray, M. M.; Soong, Y. In-Situ Infrared Study of CO₂ Adsorption on SBA-15 Grafted with γ -(Aminopropyl)triethoxysilane. *Energy Fuels* **2003**, *17*, 468.

(42) Knowles, G. P.; Graham, J. V.; Delaney, S. W.; Chaffee, A. L. Aminopropyl-functionalized Mesoporous Silicas as CO₂ Adsorbents. *Fuel Process. Technol.* **2005**, *86*, 1435.